(Received 29 April 2026, Accepted 22 May 2026, Scheduled 31 May 2026)

Characteristic Mode-Inspired Ultra-Wideband Dual-Band Notched Four-Port MIMO Antenna

Luyi Ji, Chengzhu Du*, Yongkang Yang, and Fangrui Zhang

Faculty of Artificial Intelligence, Shanghai University of Electric Power, Shanghai 200090, China

ABSTRACT: In this paper, a dual-band-notched ultra-wideband MIMO antenna fed by a microstrip line is designed. The ultra-wideband characteristics are obtained by etching a semi-elliptical notch on a circular radiation patch. For the achievement of dual-band-notched features, a U-shaped slot and an inverted U-shaped slot are employed. Additionally, the Characteristic Mode Analysis (CMA) is used to verify and analyze the notch-band and broadband characteristics. Each ground plate is connected by adding a cross-shaped branch, and a circular ring is loaded to further improve antenna isolation ($|S_{21}|$). This antenna is implemented on an FR4 substrate, and its whole size is 60 mm × 60 mm × 0.8 mm. The measured findings verify that the antenna functions within a broad bandwidth ranging 3.12–21.2 GHz (relative bandwidth 148.6%) and two frequency band rejections of 5.94–7.17 GHz and 12.49–13.92 GHz, effectively suppressing the 6G band, which belongs to the international satellite mobile communication system and the Ku band downlink. The port isolation exceeds 20 dB; the ECC is below 0.04; and the diversity gain (DG) is in excess of 9.97, all of which demonstrate the antenna's excellent diversity performance and superior radiation characteristics. The antenna is a frontrunner for next-generation wireless communication applications.

1. INTRODUCTION

The Federal Communications Commission (FCC) of the United States first approved the allocation of the Ultra-Wideband (UWB) frequency in 2002, and its operating frequency band ranges from 3.1 GHz to 10.6 GHz. Since then, UWB has become the focus in the fields of short-range high-speed communication, radar detection, and indoor positioning due to its advantages of a combination of high-speed connectivity and resilience to interference. Multiple-Input Multiple-Output (MIMO) technology offers significant enhancements to the capacity and fading resistance of communication systems without increasing bandwidth and transmits power by using spatial diversity and multiplexing gain. However, UWB (3.1–10.6 GHz) has a spectrum overlap with existing wireless communication systems, which can easily lead to mutual interference. With the continuous upgrade of mobile communication technologies, low-frequency carrier resources have gradually become scarce. The WRC (World Radio Communication Conferences)-23 has allocated the frequency band of 6.425–7.125 GHz to the international mobile communication system. In addition, the Ku-band, which is used in satellite communications, television broadcasting, and military communications, can also cause interference to communication equipment. Above all, integrating UWB antennas with notch characteristics with MIMO technology is crucial for leveraging the respective advantages of both. This can not only suppress specific frequency bands but also improve the data transmission rate.

At present, many different methods are introduced in the existing literature to obtain the characteristics of UWB. Researchers usually use a slotted-structure design [1, 2] and loaded-branch design [3, 4] to achieve the extension of the antenna's operating bandwidth. In [1], a T-shaped slot structure is etched on the antenna ground, so that the antenna generates a bandwidth of 3775 MHz at the resonant frequency of 8.95 GHz. Ref. [3] introduces a compact UWB antenna. It employs a pair of triangular branches to enhance its impedance bandwidth, while a semi-circular branch incorporated on the upper edge of the patch further extends the operating bandwidth. The optimized antenna bandwidth is 2.73–9.68 GHz. How to address inter-element mutual coupling in MIMO antennas represents a key research issue that must be faced when designing and optimizing MIMO antenna systems. The methods commonly used to improve the isolation between unit antennas include neutralization line technology [5], using Wiggly line [6], defected ground structure (DGS) [7, 8], electromagnetic band gap (EBG) structure [9, 10], and polarization diversity technology [11, 12]. Ref. [10] proposes an EBG structure to eliminate the transmission of surface waves, reduce the mutual coupling between unit antennas, and effectively improve the antenna isolation. In [11], a MIMO antenna adopts vertical diversity technology based on polarization and enhances the antenna's isolation through the integration of a cross-shaped decoupling structure. The design of notch-characteristic ultra-wideband antennas can effectively reduce the impact of other systems on ultra-wideband systems. There are many commonly used notch design methods, such as slotting the radiating patch or feeder line [13, 14], adding electromagnetic band gap (EBG) structure technology [15, 16], etching open resonant ring (SRR) technology [17], regulating the state of the PIN diode [18], asymmetric left-right extension of the ground [19], loading parasitic branches technology [20], and slotted patch

* Corresponding author: Chengzhu Du (duchengzhu@163.com).

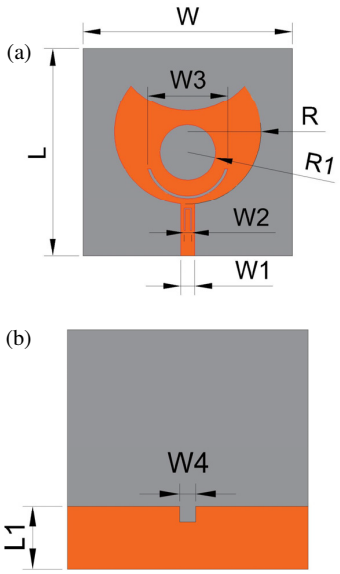

FIGURE 1. Single antenna structure. (a) Top view, (b) bottom view.

and modified ground [21–23]. Although the above MIMO antennas have good performance, it is still difficult to design MIMO antennas with high isolation characteristics under the premise of a simple structure, an ultra-wideband working bandwidth, and high selective notch characteristics.

Characteristic Mode Analysis (CMA) provides a systematic analysis method based on the intrinsic mode of the antenna, which can intuitively reveal the radiation mechanism of the antenna and guide the structural optimization [24–29]. In [24, 25], CMA is used to verify and analyze the broadband and notch-band characteristics of the antenna. The characteristic mode that contributes to the notch band is pointed out, which verifies the feasibility of the CMA to guide the antenna's design. In [26–29], CMA is employed to provide a physical interpretation of the radiation mechanisms of the proposed antenna. The radiation performance of each characteristic mode in the operating frequency range is analyzed by means of the modal saliency curve, modal current, and radiation mode.

In this paper, an ultra-wideband dual-band-notched MIMO antenna is proposed and analyzed by characteristic mode theory. A microstrip line is used to feed the antenna, and elements are placed orthogonally to obtain vertical polarization. The operating bandwidth of the antenna below -10 dB covers a range from 3.12 to 21.2 GHz. By etching U-shaped and inverted U-shaped slots on the radiation patch, the antenna generates two stopbands spanning 5.94–7.17 GHz and 12.49–13.92 GHz, thus effectively suppressing the electromagnetic interference in the 6G band and Ku standard downlink band, and is verified and analyzed by the characteristic mode theory. By adding cross-shaped branches to connect each ground plate and loading a circular ring, the antenna isolation exceeds 20 dB over the whole operating band.

The proposed antenna has the following novelties: (1) CMA is adopted to verify the notched-band and broadband characteristics. Meantime, it provides a simple structure, which is easy to process. (2) By slotting the radiation patch and the feeder line, a wider bandwidth and dual-band rejections of the 6G band and Ku standard downlink band are obtained. (3) The antenna features four ports, high isolation, good diversity performance, and ground connection.

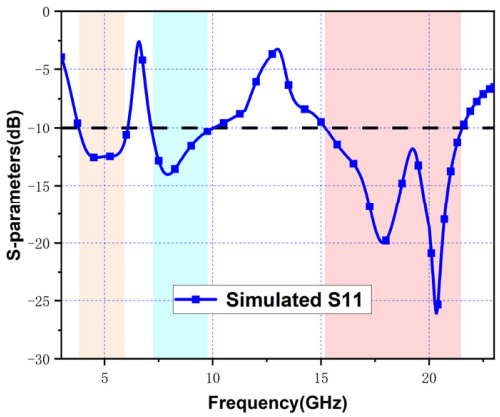

FIGURE 2. S_{11} of the antenna.

2. ANTENNA DESIGN

2.1. Single Element Antenna

The antenna designed in this paper is printed on an FR4_epoxy dielectric substrate, with a dielectric constant of 4.4 and a loss tangent of 0.02. Fig. 1 depicts the structure of the unit antenna, while the antenna's S-parameters are shown in Fig. 2. Its size is 30 mm $\times$ 30 mm $\times$ 0.8 mm, and a 50 Ω microstrip line is used for feeding. Table 1 provides the dimensional details of the unit antenna. The notch characteristic is achieved by etching two U-shaped slots, and their lengths can be calculated according to the following formulas.

$$L_{\text{U-slot}} = \frac{C}{2f_{\text{notch}}\sqrt{\varepsilon_{\text{eff}}}} \tag{1}$$

$$\varepsilon_{\text{eff}} = \frac{\varepsilon_r - 1}{2}\left(1 + 12\frac{h}{w1}\right)^{-1} + \frac{1+\varepsilon_r}{2} \tag{2}$$

In these formulas, $L_{\text{U-slot}}$ is the total length of the U-shaped slot; C denotes the light speed in a vacuum; f_{notch} represents the center frequency of the intended notch band; ε_r is the relative permittivity of the antenna dielectric substrate; ε_{eff} is the effective permittivity.

The design process of the antennas spanning from Ant-I to Ant-III is depicted in Fig. 3. Fig. 4 shows the comparison diagram of S_{11} of the antenna at different design stages. A notched

TABLE 1. Unit antenna geometric parameters.

Parameter	Dimensions/mm	Parameter	Dimensions/mm
L	30	$W1$	2
W	30	$W2$	1.06
R	10.5	$W4$	2
$R1$	4	$L1$	7.85
$W3$	11.5		

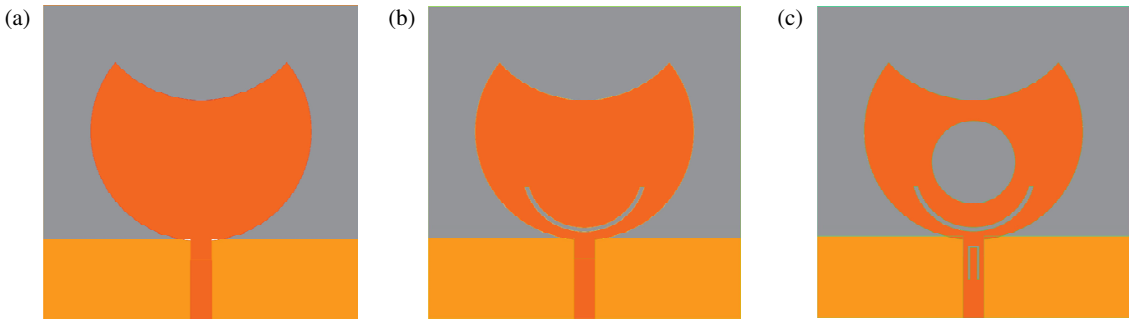

FIGURE 3. Designing process of the unitary antenna. (a) Ant-I, (b) Ant-II, (c) Ant-III.

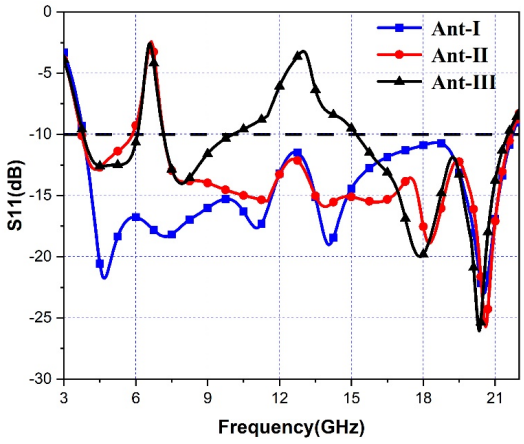

FIGURE 4. Comparison diagram of S_{11} at different design stages.

circular radiating patch forms the main structure of Ant-I, with a 50 Ω microstrip line used for feeding, and its operating frequency band is 3.85–21.72 GHz. On the basis of Ant-I, a U-shaped slot is etched on Ant-II, which achieves the notch characteristic in the frequency band of 5.86–7.16 GHz, with a bandwidth range of 3.74–21.68 GHz. Based on Ant-II, Ant-III has a reversed U-shaped slot etched at the feeder and a circular slot etched onto the radiating patch to improve the impedance matching of the antenna. The U-shaped slot etched on the radiating patch realizes the notch in the 6G frequency band, and the inverted U-shaped slot etched at the feeder generates the notch characteristic in the Ku standard frequency band. After simulation optimization, the impedance bandwidth of Ant-III spans 3.80 GHz to 21.54 GHz ,except for two notch frequency bands, which are realized at 6.07–7.16 GHz and 10.06–15.20 GHz.

2.2. Characteristic Mode Analysis of Antenna Structure

Based on the characteristic mode theory, the unit antenna is verified and analyzed by Computer Simulation Technology (CST). The curves of its Modal Significance (MS) and Characteristic Angle (CA) are shown in Fig. 5. When CA is 180°, the corresponding frequency point is the resonance point, and the MS value at this position is also equal to 1. The 22 modes of the antenna are simulated and analyzed in the frequency range of 3–22 GHz. Among them, Modes 1, 3, 4, 5, 6, 8, 9, 10, 11, 12, 13, 14, 15, 16, 17, 18, 19, 20, 21, and 22 contribute to the antenna bandwidth. Modes 2, 7, and 11 contribute to the notch band. Mode 2 mainly affects the low-frequency notch band, and Modes 7 and 11 mainly affect the high-frequency notch band. Fig. 6 shows the model significance (MS) curves of patterns 1, 2, 5, 7, 11, and 17.

Figure 6 shows the mode patterns of Modes 1 (4.9 GHz), 2 (6.39 GHz), 5 (8.57 GHz), 7 (11.3 GHz), 11 (12.83 GHz), and 17 (16.95 GHz) at their respective resonant frequencies. The resonant points corresponding to each mode correspond to the points with the MS value of 1 in this mode. As evident from the figure, the radiation patterns of Mode 2, Mode 7, and Mode 11 exhibit dips along the Z-axis, and the notched frequency bands of the antenna exactly cover 6.39 GHz, 11.3 GHz, and 12.83 GHz. In contrast, Mode 1, Mode 5, and Mode 17 correspond precisely to the three resonant frequency bands; their mode radiation patterns show no dips along the Z-axis and achieve good radiation performance. This also demonstrates the rationality of the characteristic mode analysis results.

2.3. Four-Element MIMO Antenna Development

Figure 7 depicts the structure of the proposed antenna. For the purpose of achieving vertical polarization, the four elements are arranged orthogonally, and the antenna size is 60 mm × 60 mm × 0.8 mm. By adding cross-shaped branches to connect each ground plane and loading circular rings, the antenna achieves further improvement in isolation. The operating frequency band of the antenna is 3.12–21.2 GHz, and two notch bands are realized, 5.94–7.17 GHz and 12.49–13.92 GHz, respectively, successfully suppressing the 6G band and Ku standard band downlink. Table 2 presents the geometric parameters of the antenna.

To further intuitively understand the radiation mechanism of the designed antenna, an EDA circuit simulation software is

TABLE 2. Geometric parameters of antenna.

Parameter	Dimensions/mm	Parameter	Dimensions/mm
L	60	W	60
$L1$	4	$W1$	2
$L2$	1	$R1$	3
$R2$	7	$R3$	8.5

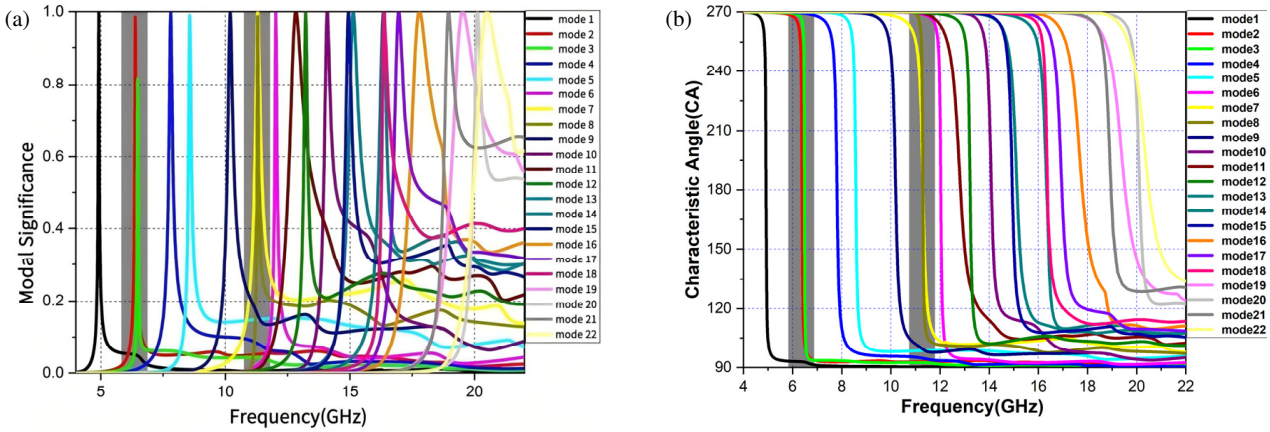

FIGURE 5. (a) MS, (b) CA.

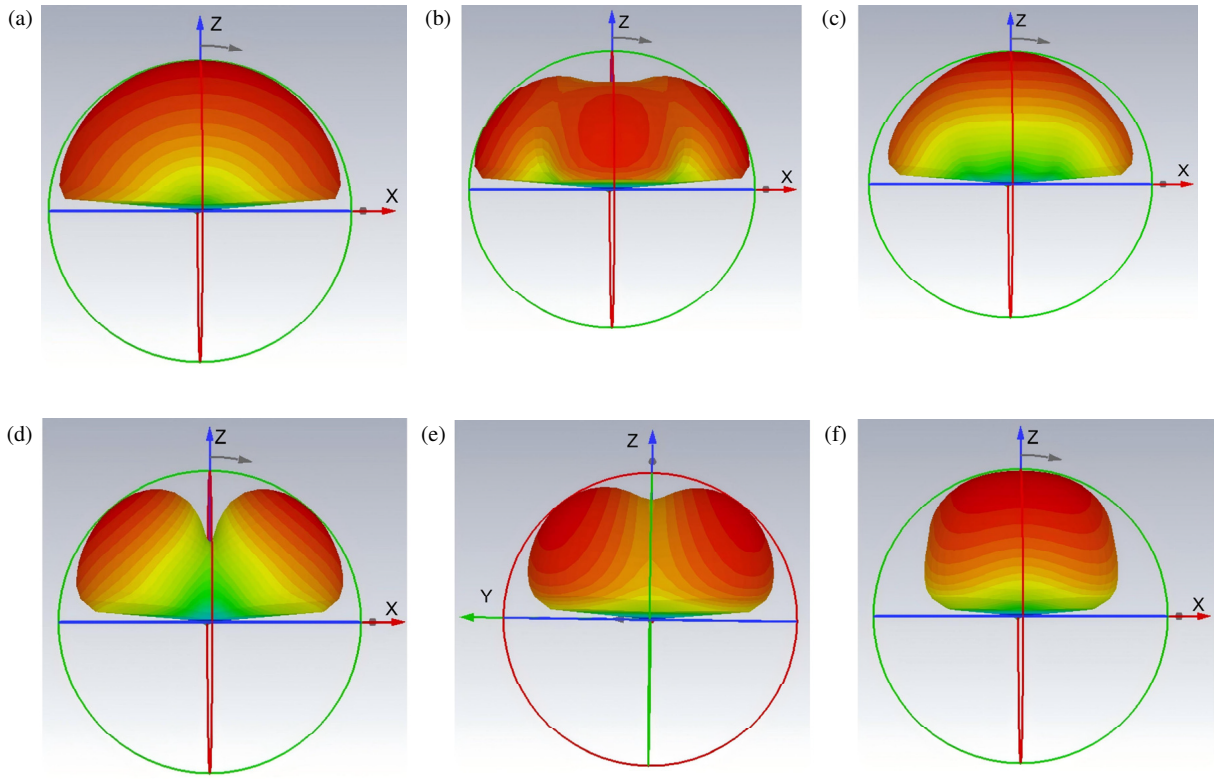

FIGURE 6. Mode patterns at different frequencies. (a) 4.9 GHz (Mode 1), (b) 6.39 GHz (Mode 2), (c) 8.57 GHz (Mode 5), (d) 11.3 GHz (Mode 7), (e) 12.83 GHz (Mode 11), (f) 16.95 GHz (Mode 17).

adopted to establish the antenna equivalent circuit model. As illustrated in Fig. 8, each antenna element adopts a series connection of resistance and inductance to match the 50 Ω feeding line. Two groups of parallel R-L-C branches are connected in series to realize the initial ultra-wideband performance. The dual-band-notched characteristics are achieved by introducing two parallel series R-L-C resonant units.

The four antenna elements share an identical lumped circuit topology. Parallel LC resonant cells are utilized to equivalently model the decoupling structure between adjacent antennas. The original coupled magnetic field is offset by additional resonant zeros, thereby achieving stable wideband resonance and high isolation.

2.4. Decoupling Structure Analysis

The antenna's design process is presented in Fig. 9, and the S parameters of the antenna in different design stages are shown in Fig. 10. The bandwidth of Antenna A is 4.5–21.4 GHz, and the band-notched bands are 6–6.9 GHz and 11.9–15.4 GHz. The bandwidth of Antenna B is 3.4–22.6 GHz, and the band-notched bands are 6.3–7.4 GHz and 11.5–14.6 GHz. The bandwidth of Antenna C is 3–22 GHz, and the band-notched bands are 5.8–7.1 GHz and 12.1–14.7 GHz.

The antenna elements in Antenna A are placed orthogonally without any isolation branches, and the ground is not connected. In the low and middle frequency bands, the impedance

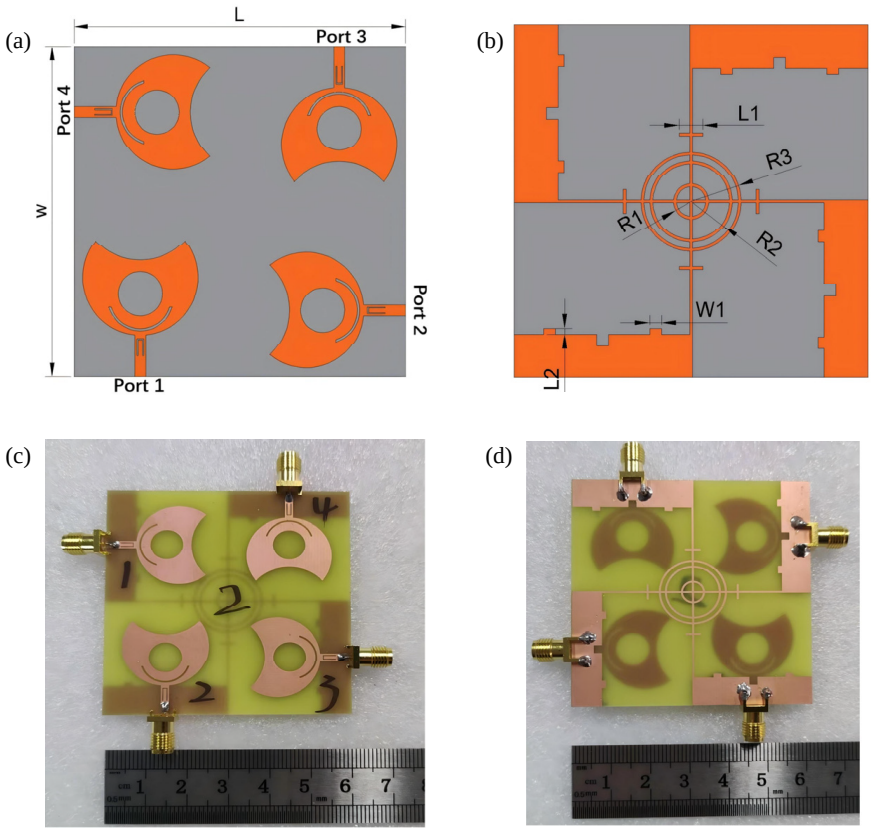

FIGURE 7. Antenna structural diagram and photograph. (a) Antenna top. (b) Antenna bottom. (c) Antenna top photograph. (d) Antenna bottom photograph.

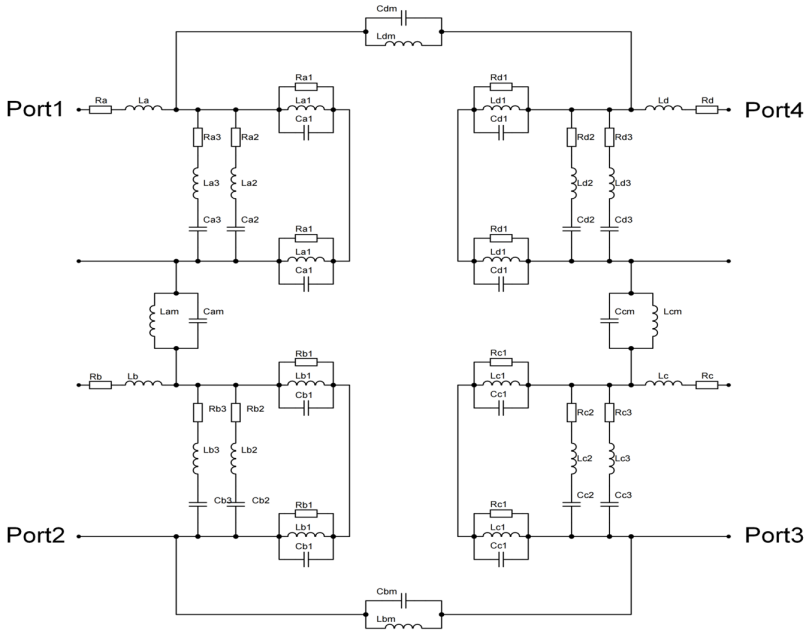

FIGURE 8. Antenna equivalent circuit model.

matching and isolation characteristics of Antenna A are found to be less than ideal. Antenna B is loaded with cross-shaped branches, and the ground is connected, which further widens the operating frequency bandwidth. At the same time, its isolation is greater than 15.2 dB. By loading three circular rings and four rectangular parasitic branches, Antenna C further enhances the antenna isolation. Across the entire frequency band, the isolation of Antenna C exceeds 20 dB.

Simulated surface current distributions of the presented antenna at 6.5 GHz, 13 GHz, and 18 GHz are depicted in Fig. 11.

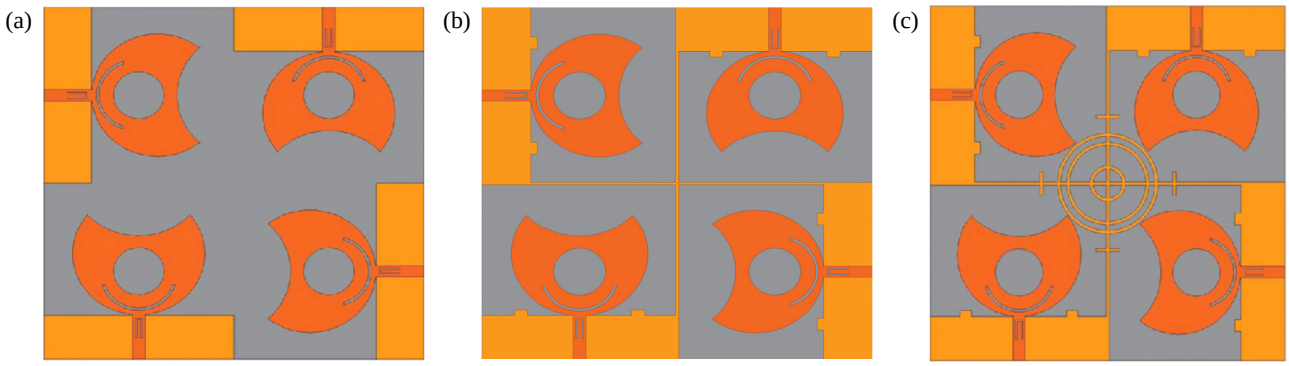

FIGURE 9. Antenna design process. (a) Antenna A, (b) Antenna B, (c) Antenna C.

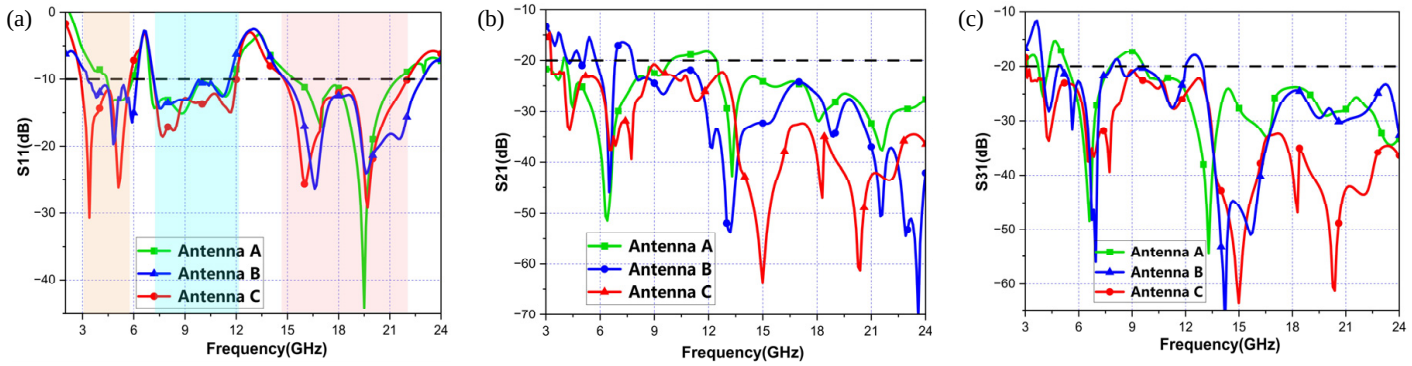

FIGURE 10. Comparison of S parameters in different design stages. (a) S_{11}, (b) S_{21}, (c) S_{31}.

The excitation signal is connected to Port 1, while other ports are all terminated with a 50 Ω load. When the operating frequency is 6.5 GHz, it can be seen from Fig. 11(a) that the surface current is mainly concentrated on feed line and the U-shaped slot; when the operating frequency is 13 GHz, Fig. 11(b) shows that the dominant current is primarily confined on the inverted U-shaped slots; at a frequency of 18 GHz, Fig. 11(c) shows that the surface current is distributed on both the circular rings and rectangular stubs. It is noteworthy that the surface current mainly flows through the primary antenna and the isolation components, which indicates that this isolation mechanism can effectively reduce the interaction between individual antennas.

3. EMPIRICAL TESTING

3.1. Scattering Parameters

Figure 12 shows the comparison between simulated and measured S-parameters of the designed antenna. Fig. 12(a) illustrates a slight left shift of the measured S_{11} curve relative to the simulated one, but within the acceptable range, it meets the design requirements. The antenna offers wide frequency coverage, spanning from 3.12 GHz to 21.2 GHz, and two notch bands are realized, which are 5.94–7.17 GHz and 12.49–13.92 GHz, respectively, successfully covering the downlink of 6G and Ku standard bands. Fig. 12(b) shows the comparison of S_{21} and S_{31} between the measured and simulated curves. The antenna's isolation is greater than 20 dB across the whole frequency band, which also shows that the four-port MIMO antenna exhibits superior isolation performance. The antenna will inevitably have errors in the process of processing and testing, so there are some subtle differences between the measured and simulated curves, but in general, it meets the design requirements.

3.2. S Parameters

Figure 13 shows the comparison of antenna S parameters at different lengths of $L1$, which is the length of the rectangular branches on the ground. In Fig. 13(a), when $L1$ is 2 mm or 6 mm, the antenna's impedance matching deteriorates in the middle frequency band, and the working bandwidth is basically not affected. When $L1$ is 4 mm, the antenna's isolation is significantly enhanced in the low-frequency band; meanwhile, the high-frequency isolation remains below −20 dB. After simulation and optimization, the value of $L1$ is selected as 4 mm.

3.3. Radiation Characteristics

Figure 14 shows the far-field test scene of the four-element MIMO antenna. Fig. 15 shows the E-plane and H-plane of the antenna at 5 GHz, 8 GHz, and 16 GHz. As illustrated in the figure, the E-plane of the simulated and measured curves presents an '8' shape, and the H-plane presents an approximately circular shape, respectively presenting bi-directional property and omnidirectional characteristic. The higher the frequency is, the more obvious the pattern distortion is. Although the testing environment is imperfect, this will cause deterioration in the high-frequency state, and the impact is within an acceptable range.

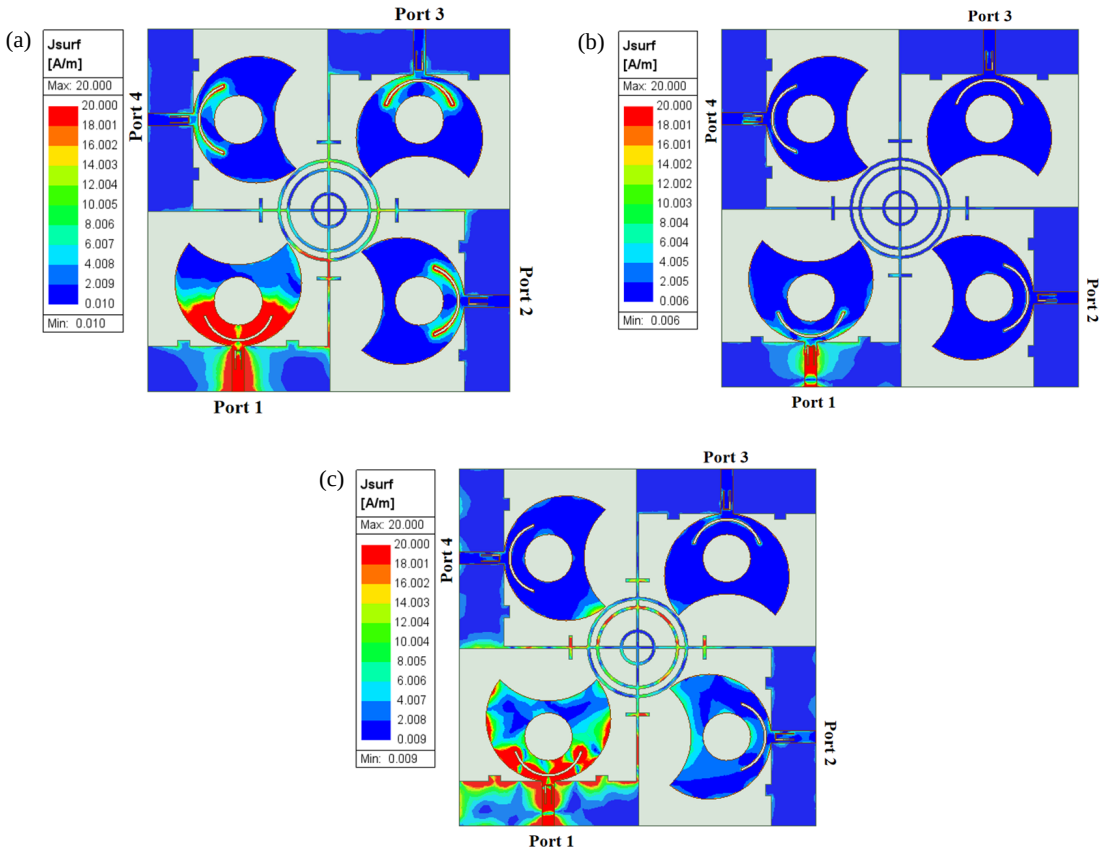

FIGURE 11. Current distributions of the proposed antenna at different frequencies. (a) 6.5 GHz, (b) 13 GHz, (c) 18 GHz.

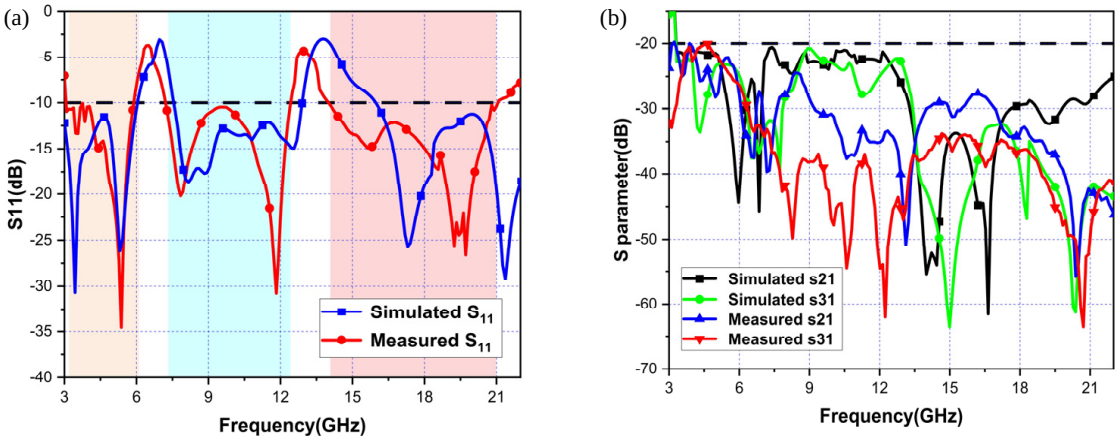

FIGURE 12. Simulated and measured S-parameters.

3.4. Antenna Gain and Efficiency

Figure 16(a) illustrates the comparison of the gain curves obtained from measurements and simulations. The proposed antenna achieves peak gains of −1.12 dB, −1.77 dB, and 5.02 dB within the operational bands of 6.6 GHz, 13 GHz, and 17 GHz, in that order. Within the band-notched frequency bands, the gain exhibits a significant drop, verifying excellent band-notched performance. The slight offset between simulated and measured results can be attributed to practical factors, including SMA connector effects, soldering quality, fabrication tolerances, and testing environmental uncertainties. It can be observed from Fig. 16(b) that the antenna achieves a radiation efficiency of around 75% across the operating bandwidth. In the notch frequency bands, the radiation efficiency decreases drastically, which verifies the superior notch characteristic.

3.5. Diversity Performance of the Antenna (ECC)

ECC is a parameter used to describe the degree of correlation between antennas, which can be calculated by formula (3).

$$\mathrm{ECC} = \frac{\left|S_{11}^{*}S_{12} + S_{21}^{*}S_{22}\right|^{2}}{\left(1 - \left|S_{11}\right|^{2} - \left|S_{21}\right|^{2}\right)\left(1 - \left|S_{22}\right|^{2} - \left|S_{12}\right|^{2}\right)} \tag{3}$$

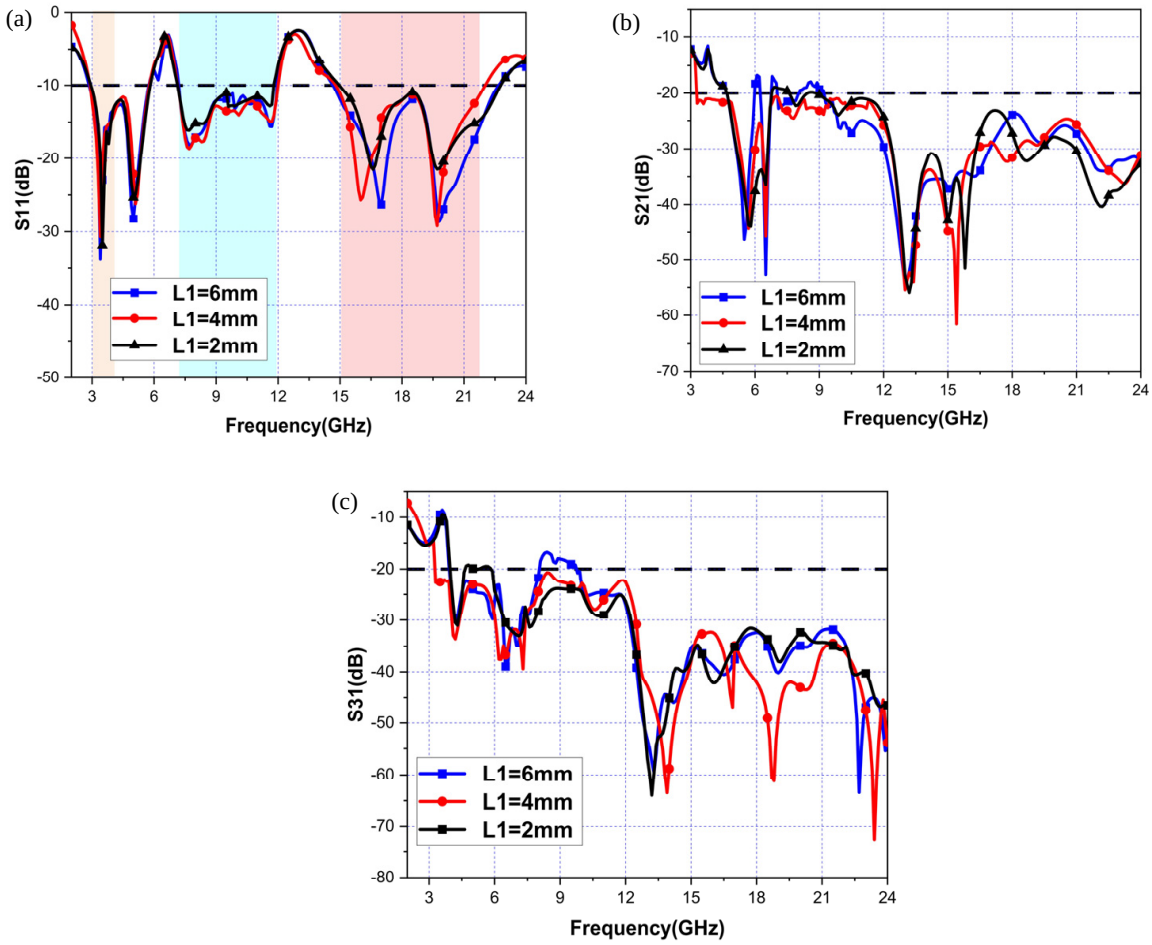

FIGURE 13. Comparison of S parameters of different sizes of $L1$. (a) S_{11}, (b) S_{21}, (c) S_{31}.

FIGURE 14. Far-field test scenario.

This formula is calculated from S-parameters. As another critical index, diversity gain (DG) is used to measure the antennas' performance, and it can be calculated by formula (4):

$$\mathrm{DG} = 10\sqrt{1 - (\mathrm{ECC})^2} \tag{4}$$

The formulas for calculating ECC from far-field parameters can be obtained from [30]. Owing to the symmetry, only the ECC and DG values of port 1, port 2, and port 3 can be tested. As can be seen from Fig. 17(a), the ECC of the antenna is less than 0.04 in the whole frequency band. As can be seen from Fig. 17(b), the DG value of the antenna is in excess of 9.97 in the whole frequency band. The MIMO antenna exhibits low element correlation and consequently good performance.

3.6. Total Active Reflection Coefficient (TARC)

TARC is an essential index used to measure the performance of the antenna in the MIMO antenna system. It evaluates the reflection characteristics of the antenna when it is excited at different ports at the same time. S-parameters are utilized for TARC's quantitative calculation. The calculation formula is as follows:

$$\mathrm{TARC} = N^{-0.5}\sqrt{\sum_{i=1}^{N}\left|\sum_{k=1}^{N} S_{ik}e^{j\theta_{k-1}}\right|^2} \tag{5}$$

Here, θ is the excitation phase angle. In this paper, four phases of 0°, 60°, 120°, and 180° are selected to study the characteristics of the MIMO antenna. Fig. 18 is the TARC simulation curve of the antenna. As the diagram shows a TARC value below -10 dB within the operating band, it can be determined that the MIMO antenna possesses superior performance.

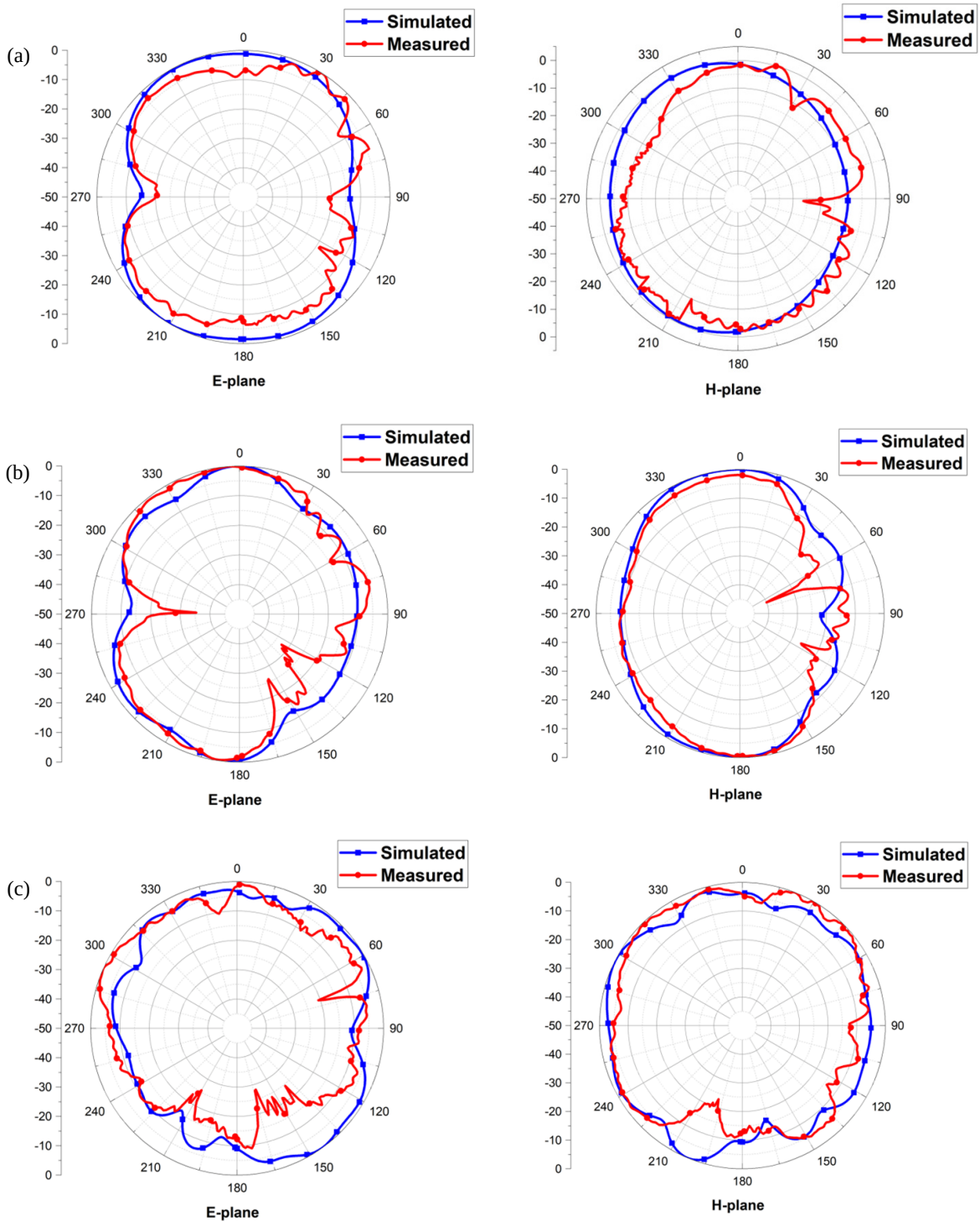

FIGURE 15. Antenna radiation pattern. (a) 5 GHz, (b) 8 GHz, (c) 16 GHz.

3.7. Channel Capacity Loss (CCL)

CCL is likewise recognized as a significant parameter for the measurement of MIMO antenna performance. In MIMO antennas, radiation performance can be deemed excellent if the CCL is less than 0.4. In formula (6), CCL is expressed as:

$$\mathrm{CCL} = -\log_2 \det(\alpha^R) \tag{6}$$

where

$$\alpha^R = \begin{bmatrix} \alpha_{11} & \alpha_{12} & \alpha_{13} & \alpha_{14} \\ \alpha_{21} & \alpha_{22} & \alpha_{23} & \alpha_{24} \\ \alpha_{31} & \alpha_{32} & \alpha_{33} & \alpha_{34} \\ \alpha_{41} & \alpha_{42} & \alpha_{43} & \alpha_{44} \end{bmatrix},$$

$$\alpha_{ii} = 1 - \left(\sum_{J=1}^{N} |S_{ij}|^2 \right),$$

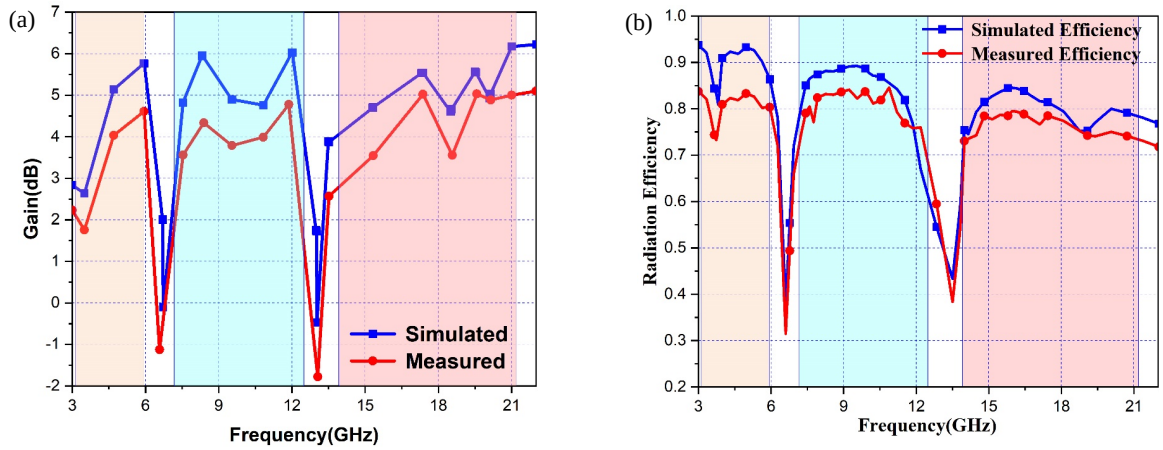

FIGURE 16. Antenna gain and efficiency. (a) Gain. (b) Efficiency.

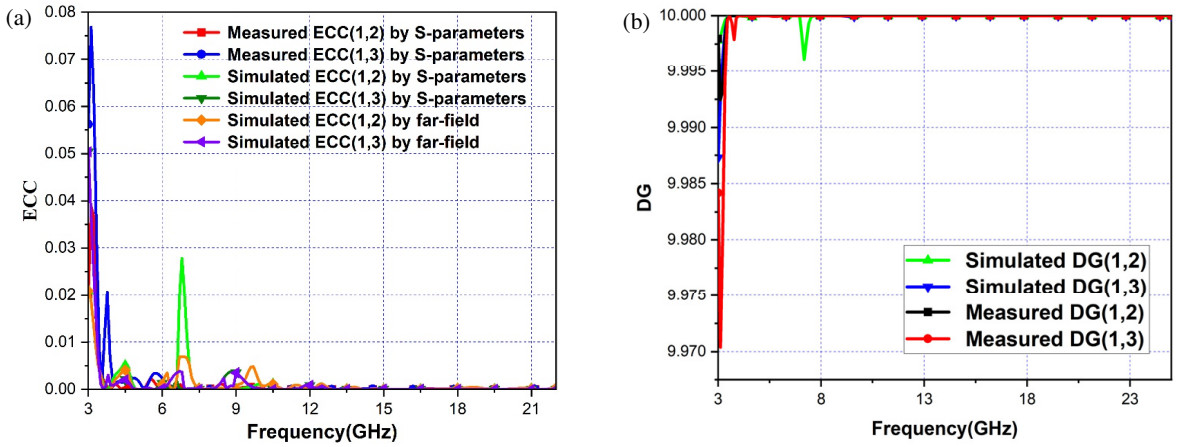

FIGURE 17. ECC and DG of the antenna. (a) ECC. (b) DG.

TABLE 3. Antenna performance comparison.

Ref.	Port	Characteristic mode analysis	Dimensions (mm^3)	Bandwidth (GHz)	Notches	Isolation (dB)	Ground connection	ECC
[21] (2025)	1	NO	$26.8 \times 26 \times 1.575$	3.15–13.57 (124.6%)	2	-	-	-
[22] (2024)	2	NO	$39 \times 18 \times 1.6$	3.1–12 (117.9%)	2	> 20	YES	< 0.18
[23] (2024)	4	NO	$40 \times 40 \times 1$	2.7–12 (126.5%)	2	> 15	NO	< 0.0002
[25] (2022)	2	YES	$21.5 \times 28 \times 1.6$	3.4–12.1 (112.3%)	2	> 16	YES	< 0.001
[26] (2024)	2	YES	$27 \times 22 \times 0.8$	3.07–11.1 (114%)	0	> 20	YES	< 0.05
[28] (2024)	4	YES	$40 \times 40 \times 1.6$	2.51–18 (151%)	0	> 20	YES	< 0.1
[29] (2025)	4	YES	$40 \times 40 \times 1.6$	3.1–11.9 (117.3%)	0	> 26	NO	< 0.016
This work	**4**	**YES**	$\mathbf{60 \times 60 \times 0.8}$	**3.12–21.2 (148.6%)**	**2**	$\mathbf{> 20}$	**YES**	$\mathbf{< 0.04}$

$$\alpha_{ij} = -\left(S_{ii}^{*} S_{ij} + S_{ji}^{*} S_{ij}\right).$$

The measured CCL value shown in Fig. 19 is obtained from measured S-parameters. Within the antenna's operating frequency band, except for notch bands, its CCL is all below 0.4 bits/s/Hz, indicating that this MIMO antenna has excellent performance.

4. ANTENNA PERFORMANCE COMPARISON

A comprehensive performance comparison between the four-port dual-notched-band antenna designed in this section and the antennas reported in existing literature is provided in Table 3. Although the antennas in [21, 22, 25] have dual notch bands, they are only single or two-element antenna designs and do not have a much wider operating bandwidth. The antenna

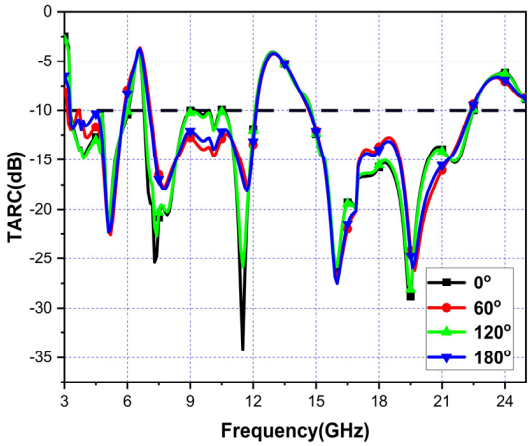

FIGURE 18. TARC of antenna.

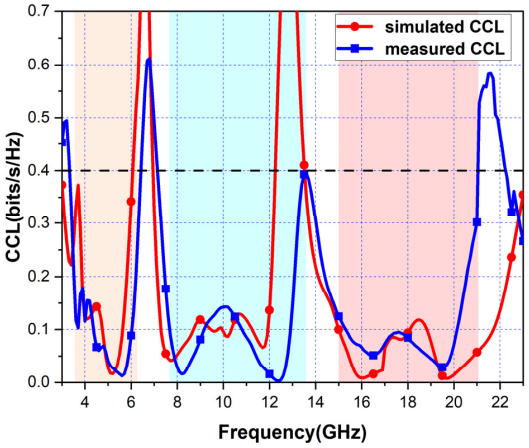

FIGURE 19. CCL of antenna.

in [23] has two notched bands; however, its ground plane is not connected, and the isolation is only less than 15 dB. CMA is adopted in [26, 28, 29], but the antenna in [26] has only two elements. The antennas in [28, 29] do not have notched bands. In general, the proposed MIMO antenna possesses the following advantages: (a) It is analyzed by CMA and is characterized by a wider bandwidth; (b) It has dual notched bands; (c) It features a high isolation level; (d) The antenna is easy to integrate with connected ground. For further improvement, a flexible antenna may be designed for wearable applications.

5. CONCLUSION

A characteristic mode-inspired ultra-wideband dual-band notched four-port MIMO antenna is proposed, and its size is $0.62\lambda_0 \times 0.62\lambda_0 \times 0.008\lambda_0$ (when the frequency is at its lowest 3.12 GHz. The corresponding wavelength is defined as λ_0). The CMA is used to verify and analyze the notched band and wideband characteristics. Two notch bands are generated by means of etching U-shaped and inverted U-shaped slots onto the radiation patch of the monopole antenna. The antenna units are arranged in an orthogonal configuration, and the isolation effect is improved by loading cross, ring, and rectangular isolation branches. The antenna has a wide measured bandwidth covering 3.12 to 21.2 GHz. The notch bands are 5.94–7.17 GHz and 12.49–13.92 GHz, successfully suppressing the 6G band and Ku standard band. The antenna isolation exceeds 20 dB, covering the whole operating band. As key parameters, the ECC value falls below 0.04, and the DG value surpasses 9.97. The designed antenna can be applied to ultra-wideband high-speed communication systems and Internet of Things (IoT) communication. To accommodate the growing demand for wearable devices, the antenna can be designed by adopting flexible materials in future research.

REFERENCES

[1] Zadehparizi, F., "Design of low-profile SWB monopole antenna with band-notched characteristics," *AEU — International Journal of Electronics and Communications*, Vol. 198, 155865, 2025.

[2] Alazemi, A. J. and Y. T. Alsaleh, "An ultrawideband antenna with two independently tunable notch bands," *Alexandria Engineering Journal*, Vol. 79, 402–410, 2023.

[3] Ali, E. M., W. A. Awan, M. S. Alzaidi, A. Alzahrani, D. H. Elkamchouchi, F. Falcone, and S. S. M. Ghoneim, "A shorted stub loaded UWB flexible antenna for small IoT devices," *Sensors*, Vol. 23, No. 2, 748, 2023.

[4] Wang, M., J. Nan, and J. Liu, "High-isolation UWB MIMO antenna with multiple X-shaped stubs loaded between ground planes," *International Journal of Antennas and Propagation*, Vol. 2021, No. 1, 1155471, 2021.

[5] Kapure, V. R. and S. S. Rathod, "A two element EBG-inspired UWB MIMO antenna with triple band notched characteristics and high isolation," *Sādhanā*, Vol. 48, No. 1, 7, 2023.

[6] Chaudhary, A. K. and M. Manohar, "A quadruple band-notched SWB MIMO antenna with enhanced isolation using wiggly line," *Radioengineering*, Vol. 33, No. 2, 274–281, 2024.

[7] Ding, T., H. Yang, Z. Chen, Z. Lin, B. He, and C.-Z. Han, "A 4-element UWB MIMO antenna system with high isolation performance," *Applied Computational Electromagnetics Society Journal (ACES)*, Vol. 38, No. 10, 799–806, 2023.

[8] Zhao, L., Y. Wang, C. Liu, D. Song, C. Hu, C. Li, H. Zhao, and Z. Wang, "Compact circular-shaped MIMO antenna covers UWB bandwidth with four frequently-used band-notched characteristics for multi-scenario applications," *IEEE Access*, Vol. 12, 32 762–32 771, 2024.

[9] Tang, Y., T. Wang, J. Zheng, Z. Lyu, X. Tian, and J. Mou, "Mutual coupling suppression of MIMO array with non-uniform curved-strip EBG structure via shape and layout co-optimization," *AEU — International Journal of Electronics and Communications*, Vol. 178, 155306, 2024.

[10] Pakala, R. and R. Dasari, "Mutual coupling reduction in UWB-MIMO antenna using circular slot EBG structure," *Progress In Electromagnetics Research M*, Vol. 119, 177–188, 2023.

[11] Jayant, S. and G. Srivastava, "Close-packed quad-element triple-band-notched UWB MIMO antenna with upgrading capability," *IEEE Transactions on Antennas and Propagation*, Vol. 71, No. 1, 353–360, 2023.

[12] Ka'bi, A. A., "Planar MIMO antenna model for spectrum sensing applications," *Wireless Personal Communications*, Vol. 135, No. 2, 919–939, 2024.

[13] Addepalli, T., C. J. Rani, P. Nimmagadda, P. Badugu, J. B. Kamili, C. M. Kumar, P. Sunitha, and B. K. Kumar, "Design

and analysis of UWB antenna with triple band notched characteristics verified with TCM analysis," *Wireless Personal Communications*, Vol. 134, No. 3, 1641–1664, 2024.

[14] Shekhawat, S. S., D. Lodhi, and S. Singhal, "Dual band notched superwideband MIMO antenna for 5G and 6G applications," *AEU — International Journal of Electronics and Communications*, Vol. 184, 155419, 2024.

[15] Abbas, A., N. Hussain, M. A. Sufian, W. A. Awan, J. Jung, S. M. Lee, and N. Kim, "Highly selective multiple-notched UWB-MIMO antenna with low correlation using an innovative parasitic decoupling structure," *Engineering Science and Technology, An International Journal*, Vol. 43, 101440, 2023.

[16] Mukherjee, S., A. Roy, A. Mukherjee, S. Kundu, P. P. Sarkar, and S. Bhunia, "Notch band characteristics improvement of a printed ultra wideband antenna by embedding frequency selective surface," *AEU — International Journal of Electronics and Communications*, Vol. 178, 155276, 2024.

[17] Saleem, S., S. Kumari, V. Mirdha, D. Yadav, and D. Bhatnagar, "Circular split ring resonator (SRR) slot and ground stub based slotted circular ultra-wideband MIMO antenna with WLAN band exclusion and high isolation performance," *Sādhanā*, Vol. 49, No. 1, 26, 2024.

[18] Saleem, S., S. Kumari, D. Yadav, M. G. Siddiqui, and D. Bhatnagar, "A planar UWB-MIMO antenna with high isolation and reconfigurable single band-elimination characteristics," *AEU — International Journal of Electronics and Communications*, Vol. 170, 154853, 2023.

[19] Biswas, A. K., S. Biswas, S. Haldar, and A. Nandi, "A highly decoupled flexible 4-element MIMO antenna with band notched characteristics for ultra wide-band wearable applications," *AEU — International Journal of Electronics and Communications*, Vol. 173, 154985, 2024.

[20] Hemalatha, T. and B. Roy, "Ground plane alteration extremely wideband SPAS pair-based MIMO antenna with improved isolation and band notched characteristics," *AEU — International Journal of Electronics and Communications*, Vol. 176, 155118, 2024.

[21] Paul, S., S. Rana, A. R. Azad, D. Nandi, and A. Mohan, "Compact planar UWB microstrip antenna with independently controllable dual notch bands," *ETRI Journal*, Vol. 47, No. 6, 1125–1138, 2025.

[22] Banerjee, J., A. Gorai, and R. Ghatak, "Development and investigation of a compact band-notched MIMO antenna attaining wideband isolation for UWB applications," *Journal of Electromagnetic Waves and Applications*, Vol. 38, No. 11, 1283–1299, 2024.

[23] Addepalli, T., V. S. Nagaraju, M. Kilaru, G. N. Kumar, J. B. Kamili, C. M. Kumar, P. Nimmagadda, and B. K. Kumar, "A compact self isolated UWB-MIMO antenna with WiMAX and WLAN band notched characteristics for portable wireless applications," *Wireless Personal Communications*, Vol. 135, No. 3, 1363–1382, 2024.

[24] Rao, B. R., K. S. Chakradhar, and D. Nataraj, "Design, optimization and experimental verification of UWB-MIMO antenna with WLAN and complete X-band notched characteristics, checked with characteristic mode analysis (CMA)," *Analog Integrated Circuits and Signal Processing*, Vol. 115, No. 1, 139–158, 2023.

[25] Kumar, P., T. Ali, and M. P. Mm, "Characteristic mode analysis-based compact dual band-notched UWB MIMO antenna loaded with neutralization line," *Micromachines*, Vol. 13, No. 10, 1599, 2022.

[26] Li, W., L. Wu, S. Li, X. Cao, and B. Yang, "Bandwidth enhancement and isolation improvement in compact UWB-MIMO antenna assisted by characteristic mode analysis," *IEEE Access*, Vol. 12, 17 152–17 163, 2024.

[27] Xiao, B. and H. Wong, "Whole sub-6 GHz multi-order-dual-degenerate-modes loop antenna in mobile smart devices for IoT applications," *IEEE Internet of Things Journal*, Vol. 12, No. 16, 33 144–33 154, 2025.

[28] Ghosh, P., A. Gorai, S. Behera, and R. Ghatak, "Design of compact UWB antenna using characteristic mode analysis and its quad-port MIMO realization with novel isolation technique," *Journal of Electromagnetic Waves and Applications*, Vol. 38, No. 4, 443–459, 2024.

[29] Suresh, A. C., C. Althi, O. P. Kumar, M. Alathbah, B. Madhav, *et al.*, "Modal analysis-based ultrawideband 4×4 MIMO antenna with flower configuration," *AEU — International Journal of Electronics and Communications*, Vol. 192, 155685, 2025.

[30] Zhang, J., C. Du, and R. Wang, "Design of a four-port flexible UWB-MIMO antenna with high isolation for wearable and IoT applications," *Micromachines*, Vol. 13, No. 12, 2141, 2022.